Energy Dissipation due to Capillary Interactions: Hydrophobicity Maps in Force Microscopy

E. Sahagún,[1] P. García-Mochales,[1] G. M. Sacha,[2] and J. J. Sáenz[1]

[1]*Departamento de Física de la Materia Condensada and Instituto "Nicolás Cabrera," Universidad Autónoma de Madrid, E-28049 Madrid, Spain*

[2]*Materials Science Division, Lawrence Berkeley National Laboratory, University of California, Berkeley, California 94720, USA*

(Received 16 November 2006; published 27 April 2007)

The energy dissipation process involved in the formation and rupture of a nanometer-sized capillary-condensed water bridge is theoretically analyzed. With the help of numerical simulations, the dissipation contrast in amplitude-modulated atomic force microscopy is shown to be a result of a nontrivial interplay between the energy dissipated in each rupture process and the bistable motion of the cantilever. In the repulsive high amplitude regime, the dissipated power is a function of the tip and sample contact angles being independent of the elastic properties of the system. Working in this regime, energy dissipation images in air can be regarded as surface hydrophobicity maps.

DOI: 10.1103/PhysRevLett.98.176106 PACS numbers: 68.37.Ps, 07.79.Lh, 47.55.nk, 87.64.Dz

Atomic force microscopy (AFM) has become a standard tool to image and manipulate surfaces with nanometer resolution. In order to minimize sample deformations due to the tip interaction, AFM images are usually taken by using different dynamic operation modes [1]. Phase contrast images, obtained by recording the phase lag of the cantilever oscillation relative to the driving signal [2], often provide significantly more contrast than the topographic image. At a fixed feedback amplitude, phase shift variations are directly linked to energy dissipation processes [3–5]. However, most of the phase and energy dissipation images are purely qualitative, mainly due to the absence of simple relationships relating phase changes and energy dissipation with specific surface properties.

Under air ambient conditions, the phase contrast is strongly influenced by capillary forces [6–8]. When the tip approaches the sample, water condensation can induce the formation of a nanometer-sized water bridge. The relevance of liquid bridges for both imaging and nanofabrication have driven numerous experimental [6–11] and theoretical [8,12,13] efforts to understand nanometer-sized systems involving capillaries. Understanding capillary contrast in AFM maps would be particularly interesting for biological applications [14], where the recognition of different species is frequently based on their hydrophilic or hydrophobic nature [6,8,14].

In this Letter, we present a theoretical analysis of the energy dissipation involved in the formation and rupture of capillary-condensed water bridges. Based on a simple model, we predict a quantitative relation between the energy dissipated U_{dis} and tip and sample contact angles and relative humidity (RH). One could naively argue that the averaged power dissipated by capillary forces in amplitude-modulated AFM (AM-AFM) would simply be given by $P_{\mathrm{dis}} \approx U_{\mathrm{dis}}\omega/(2\pi)$, i.e., the energy dissipated per oscillation times the number of oscillations per unit time. However, as we will show, this is, in general, not true. The dissipation contrast is a result of a nontrivial interplay between the energy dissipated in each rupture process and the bistable motion of the cantilever [1,15–17]. AM-AFM presents two regimes of operation: the *attractive* (AR) and the *repulsive* (RR) regimes [16] (also known as low and high amplitude regimes [17]). As we will see, only in the RR does the tip hit the surface in each oscillation. The dissipated power is then a function of the tip and sample contact angles being independent of the elastic properties of the system. As a consequence, only when working in the RR can energy dissipation images of biological samples in air be regarded as surface hydrophobicity maps.

We shall consider a simplified model (sketched in Fig. 1), keeping only the main ingredients for capillary condensation. Our model does not include possible effects

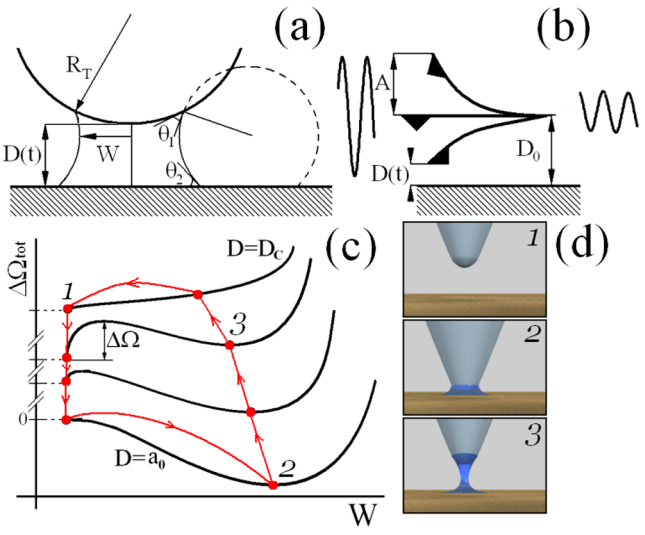

FIG. 1 (color online). (a) Sketch of the water bridge geometry. (b) Tip-cantilever-driver system. (c) Schematic representation of the formation or rupture process in tapping mode. (d) Graphic representation of water neck formation or rupture.

related to nanostructured water or adsorbed icelike water on the surface [18] which could be important at low humidities [19,20]. The homogeneous liquid meniscus is assumed to have a constant curvature radius. For a given tip radius R_T and a tip-sample distance D, the pendular ring geometry of the bridge [see Fig. 1(a)] is characterized by the tip and sample contact angles θ_1 and θ_2, respectively, and the bridge width W. The "excess" grand potential [13,21] $\Delta\Omega_{\rm tot}$ to condense the water bridge is given by the sum of surface and volume contributions. The surface energy term is given by $\Delta\Omega_S = S_{\rm LV}\gamma_{\rm LV} + S_{\rm LS}(\gamma_{\rm LS} - \gamma_{\rm VS}) + S_{\rm LT}(\gamma_{\rm LT} - \gamma_{\rm VT}) = \gamma[S_{\rm LV} - S_{\rm LS}\cos(\theta_2) - S_{\rm LT} \times \cos(\theta_1)]$, where the S's are the surface areas (the γ's are the surface energies) of the liquid-vapor (LV), liquid-sample (LS), liquid-tip (LT), vapor-sample (VS), and vapor-tip (VT) interphases ($\gamma \equiv \gamma_{\rm LV}$). At a given temperature T, the condensation energy of water molecules from air is proportional to the bridge volume V:

$$\Delta\Omega_V = \gamma V\left(\frac{RT}{\gamma\vartheta_m}\ln(1/H)\right) \equiv \gamma V\frac{1}{r_k}, \qquad (1)$$

where ϑ_m is the molar volume, $R = 8.31\ \mathrm{J\,mol^{-1}\,K^{-1}}$, H is the relative humidity, and r_k is (the absolute value of) the Kelvin radius ($RT/\{\gamma\vartheta_m\} = 1.85\ \mathrm{nm^{-1}}$ for water at 20 °C). Figure 1(c) shows typical $\Delta\Omega_{\rm tot}$ vs W curves for different tip-sample distances. For D smaller than a critical distance D_C, the grand potential vs W presents a local maximum $\Delta\Omega^\dagger(D)$ (which corresponds to the nucleation free energy barrier [13]) and a minimum at $W = W_0(D)$ [with $\Delta\Omega_{\rm tot} = \Delta\Omega_0(D)$], corresponding to a liquid bridge in mechanical equilibrium.

The hysteresis associated to the formation and rupture of a liquid bridge is sketched with arrows in Fig. 1(c). At distances larger than $D_C \approx r_k(\cos\theta_1 + \cos\theta_2)$, there is no water bridge. As the tip approaches the sample, the nucleation free energy barrier decreases, and capillary condensation can take place. However, since capillary condensation is a thermal-activated process, the condensation time $\tau \propto \exp(\Delta\Omega^\dagger/k_BT)$ should be shorter than the typical time $\tau_{\rm contact}$ spent by the AFM tip in close proximity to the sample (of the order of microseconds for typical tapping frequencies). Although the understanding of the dynamics of the process is still very incomplete [22], recent friction force microscopy experiments [23] suggest that the nucleation time of nanoscale water bridges is of the order of milliseconds at 40% RH. Since $\Delta\Omega^\dagger$ strongly depends on the RH [13], this result would imply condensation times below microseconds only for RH larger than 50%.

When the tip retracts, the condensed water bridge elongates and breaks at $D \approx D_C$. Assuming that the neck evolves in thermodynamic equilibrium, the capillary force is simply given by $F_{\rm cap}(D) = -\partial\Delta\Omega_0/\partial D$. Since the tip-sample contact corresponds to $D = a_0$ (a_0 being an intermolecular distance [9,24]), the total energy dissipated by the tip-cantilever system in each condensation-rupture cycle would be [25]

$$U_{\rm dis} \approx \Delta\Omega_0(D_C) - \Delta\Omega_0(a_0). \qquad (2)$$

The energy dissipated can be easily calculated for a large tip radius ($R_T \gtrsim \mu$m) where the bridge width is much larger than the Kelvin radius. In this limit, the capillary force can be approximated by [9,10]

$$F_{\rm cap} = 2\pi R_T\gamma\chi(1 - D/D_C) \quad \text{for} \quad a_0 < D < D_C \qquad (3)$$

and zero otherwise. Here $\chi \equiv (\cos\theta_1 + \cos\theta_2)$ (notice that indentation into the sample does not change appreciably the equilibrium energy; this leads to zero capillary force for $D < a_0$). The corresponding dissipated energy

$$U_{\rm dis} \approx \pi r_k R_T\gamma(\chi - a_0/r_k)^2 \qquad (4)$$

is directly related to the sample hydrophobicity [through $(\chi - a_0/r_k)^2$]. For nanoscale tip radii, the equilibrium equations are not linear, and there are no simple closed expressions for $F_{\rm cap}$ and $U_{\rm dis}$. However, as shown in Fig. 2, the numerical results for $U_{\rm dis}$ obtained directly from Eq. (2) show that, even for the smallest tip radius, $U_{\rm dis}$ can still be adjusted to an expression of the form $U_0(\chi - \chi_0)^2$. It is worth noticing that the adhesion force $F_{\rm cap}(a_0)$ fails to describe the dependence on the RH of nanotip AFM adhesion experiments on some hydrophilic surfaces at low RH ($\lesssim 40\%$) [19,24,26,27], possibly due to the presence of adsorbed icelike structured water [19].

Let us now discuss the dynamic response of the AFM in the presence of capillary phenomena. The usual theoretical approach [1,17,28,29] describes the system as a driven anharmonic oscillator [Fig. 1(b)] including the cantilever elastic response, the hydrodynamic damping with the medium, and the tip-sample interaction forces $F_{\rm ts}$. In order to describe $F_{\rm ts}$, we include both van der Waals and Dejarguin-Muller-Toporov [9,30] contact forces as discussed in Refs. [17,31], plus the contribution of capillary forces

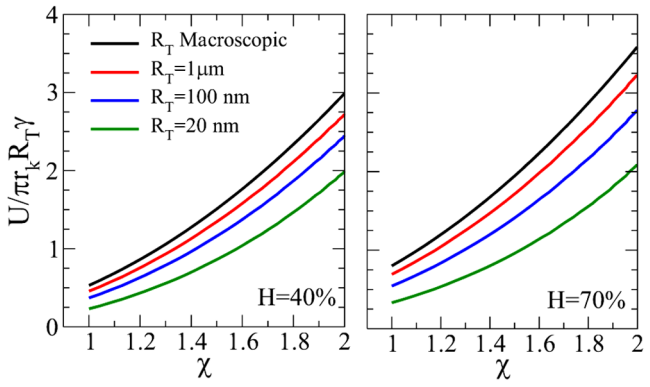

FIG. 2 (color online). Energy dissipated in the rupture of a liquid bridge vs the average contact angle $\chi \equiv (\cos\theta_1 + \cos\theta_2)$ for different tip radius and relative humidities. The tip contact angle is assumed to be constant ($\theta_1 = 0$). As R_T increases, the energy approaches the macroscopic result given in Eq. (4).

F_{cap} obtained from the numerical minimization of $\Delta\Omega_{tot}$ (the effect of other hysteretic contact forces, such as those arising in very soft samples, has been described in Ref. [29]). The averaged oscillation amplitude A and the phase shift ϕ are obtained by means of Fourier transform of the numerical amplitude vs time curves using a 100 μs time window. While A and ϕ can be acquired directly from the experiment, P_{dis} must be calculated indirectly. Assuming cantilever sinusoidal motion, P_{dis} can be obtained from [3]

$$P_{dis} = \frac{k\omega}{2Q}\left[A_0 A \sin\phi - A^2\frac{\omega}{\omega_0}\right], \quad (5)$$

A_0 being the free oscillation amplitude, ω_0 the free resonance frequency, k the spring constant of the cantilever, and Q the quality factor. The average dissipated power obtained directly from the numerical simulations is in perfect agreement with Eq. (5).

Our numerical results are summarized in Fig. 3, where we plot the typical behavior of the phase shift and dissipated power vs the normalized amplitude A/A_0. Phase shift curves [Figs. 3(a) and 3(c)] are particularly useful to identify the different operating regimes in tapping mode [1,17] and are similar to those obtained without capillary interactions. When the averaged tip-sample distance (D_0) is large, the cantilever oscillates with the free amplitude $A/A_0 = 1$. Working at $\omega = \omega_0$, the oscillation has an initial phase lag of 90° with respect to the driving force. As D_0 decreases, the amplitude decreases, and there is a continuous growth of the phase ϕ. This region, where $\phi > 90°$, corresponds to the AR [1]. The corresponding dissipated power P_{dis} [shown in Figs. 3(b) and 3(d)] presents a maximum with respect to the amplitude ratio in full agreement with recent experimental results [32].

The maximum in the dissipated power has been associated with the existence of hysteresis in the long range interaction forces [32] or with viscoelastic interactions [33]. As shown in Fig. 3(d), capillary interactions (in general, any contact interaction leading to surface energy hysteresis) may also lead to a maximum in the AR: Dissipation takes place once the closest tip-surface distance goes below a critical distance ($D_{min} \leq a_0$ in our model). Since the energy lost in each contact breaking process is constant, changes in the dissipated power arise as a consequence of a beating phenomenon [6]: After the breaking process, the cantilever, which has less energy than before, will not reach the same amplitude as before the impact, and the tip may not hit the sample surface during the next swings. As D_0 decreases, the time delay between two contacts decreases, and, as a consequence, dissipation increases. The maximum in the dissipated power correlates with a minimum in the averaged value of D_{min} with respect to the amplitude ratio. In the AR, the maximum dissipated power depends not only on the capillary interactions but also on the elastic properties of both the cantilever and the sample. It will then be difficult to interpret power dissipation contrast in heterogeneous samples.

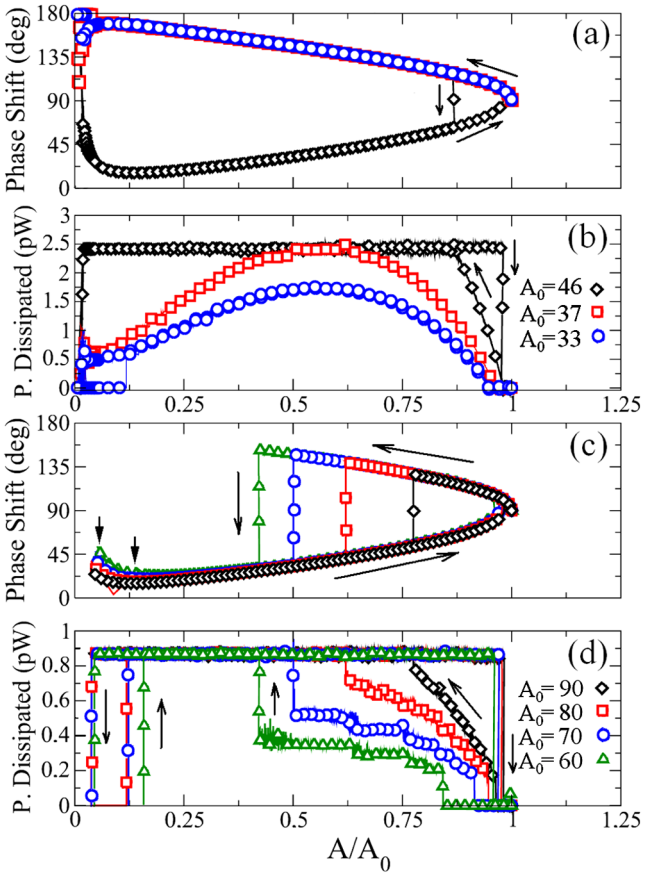

FIG. 3 (color online). (a) Phase and (b) power dissipated vs normalized amplitude. The cantilever parameters are $k = 27.5$ N/m, $Q = 400$, $\nu \equiv \omega_0/(2\pi) = 280$ kHz. (c),(d) are the same as (a),(b) but for higher amplitudes (and different cantilever constants: $k = 2$ N/m, $Q = 100$, $\nu = 100$ kHz). In the RR ($\phi < 90°$), the energy dissipated per oscillation is simply given by U_{dis}.

Abrupt changes in the phase from values above to below 90° correspond to the transition from AR to RR. These jumps, and the associated hysteresis [16], arise as a consequence of the bistable motion of the cantilever [15,34]. The transition is usually marked by a discontinuous jump in the dissipated power. Although the oscillation is chaotic in the high amplitude regime [35], the tip, at the closest distance, is always in (repulsive) contact with the sample, and there is a condensation-rupture cycle for each oscillation. This is a very important result since, once the system is in the RR, P_{dis} does not depend on the amplitude and saturates to the theoretical limit. In this regime, the energy dissipated per oscillation coincides with U_{dis} and is independent of the amplitude and elastic properties of the system. This is a general result that does not depend on the details of the liquid bridge model. The dependence of U_{dis} on RH and θ_1 and θ_2 (Fig. 2) could be experimentally

checked by measuring the energy dissipated per oscillation in the RR.

In summary, we have shown that capillary dissipation contrast in AM-AFM strongly depends on the operation regime. Only in the RR is the energy dissipated per oscillation independent on the amplitude and elastic properties of the system. For a given tip and RH, the dissipated power is just a function of the sample contact angle. As a consequence, only when working in the repulsive regime can energy dissipation images of biological samples in air be regarded as surface hydrophobicity maps.

We thank S. Albadalejo, P. J. de Pablo, J. Gómez, L. Froufe, M. Laroche, K. Leslye, M. Salmeron, A. Valbuena, and C. Wyman for interesting discussions. This work was supported by the Spanish No. FIS2005-05137 and No. NAN2004-09183-C10-05 and Microseres-CM and the EU-IP "Molecular Imaging" (No. LSHG-CT-2003-503259).

[1] R. García and R. Pérez, Surf. Sci. Rep. **47**, 197 (2002).
[2] D. Chernoff, *Proceedings: Microscopy and Microanalysis* (Jones and Bergell, New York, 1995), p. 888.
[3] J. P. Cleveland *et al.*, Appl. Phys. Lett. **72**, 2613 (1998).
[4] J. Tamayo and R. García, Appl. Phys. Lett. **73**, 2926 (1998).
[5] P. D. Ashby and C. M. Lieber, J. Am. Chem. Soc. **127**, 6814 (2005).
[6] S. J. T. van Noort *et al.*, Ultramicroscopy **69**, 117 (1997).
[7] M. Luna, J. Colchero, and A. M. Baró, Appl. Phys. Lett. **72**, 3461 (1998); A. Gil *et al.*, Langmuir **16**, 5086 (2000).
[8] L. Zitzler, S. Herminghaus, and F. Mugele, Phys. Rev. B **66**, 155436 (2002).
[9] J. Israelachvili, *Intermolecular and Surface Forces* (Academic, San Diego, 1991).
[10] T. Thundat *et al.*, Surf. Sci. Lett. **294**, L939 (1993).
[11] R. L. Fisher and J. Israelachvili, J. Colloid Interface Sci. **80**, 528 (1981); M. Binggeli and C. M. Mate, Appl. Phys. Lett. **65**, 415 (1994); M. Schenk, M. Füting, and R. Reichelt, J. Appl. Phys. **84**, 4880 (1998); R. Guckenberger *et al.*, Science **266**, 1538 (1994); R. García, M. Calleja, and H. Rohrer, J. Appl. Phys. **86**, 1898 (1999); R. D. Piner *et al.*, Science **283**, 661 (1999); E. Riedo, F. Lévy, and H. Brune, Phys. Rev. Lett. **88**, 185505 (2002).
[12] R. G. Horn, J. Am. Ceram. Soc. **73**, 1117 (1990); J. Y. Yuan, Z. Shao, and C. Gao, Phys. Rev. Lett. **67**, 863 (1991); A. Valencia, M. Brinkman, and R. Lipowsky, Langmuir **17**, 3390 (2001); C. Gao, Appl. Phys. Lett. **71**, 1801 (1997); A. de Lazzer, M. Dreyer, and H. J. Rath, Langmuir **15**, 4551 (1999); S. Gómez-Moñivas *et al.*, Phys. Rev. Lett. **91**, 056101 (2003); G. M. Sacha, A. Verdaguer, and M. Salmeron, J. Phys. Chem. B **110**, 14 870 (2006).
[13] F. Restagno, L. Bocquet, and T. Biben, Phys. Rev. Lett. **84**, 2433 (2000).
[14] H. G. Hansma and J. Hoh, Annu. Rev. Biophys. Biomol. Struct. **23**, 115 (1994); Z. Shao *et al.*, Adv. Phys. **45**, 1 (1996); M. Stark *et al.*, Biophys. J. **80**, 3009 (2001); A. Janiijevi, D. Ristic, and C. Wyman, J. Microsc. **212**, 264 (2003).
[15] P. Gleyzes, P. K. Kuo, and A. C. Boccara, Appl. Phys. Lett. **58**, 2989 (1991).
[16] B. Anczykowski, D. Krüger, and H. Fuchs, Phys. Rev. B **53**, 15 485 (1996).
[17] R. García and A. San Paulo, Phys. Rev. B **60**, 4961 (1999).
[18] A. Verdaguer *et al.*, Chem. Rev. **106**, 1478 (2006).
[19] D. B. Asay and S. H. Kim, J. Chem. Phys. **124**, 174712 (2006).
[20] K. B. Jinesh and J. W. M. Frenken, Phys. Rev. Lett. **96**, 166103 (2006).
[21] R. Evans, in *Liquids and Interfaces*, edited by J. Charvolin, J. F. Joanny, and J. Zinn-Justin (Elsevier, New York, 1989).
[22] L. Bocquet *et al.*, Nature (London) **396**, 735 (1998); N. Maeda, J. N. Israelachvili, and M. M. Kohonen, Proc. Natl. Acad. Sci. U.S.A. **100**, 803 (2003).
[23] R. Szoszkiewicz and E. Riedo, Phys. Rev. Lett. **95**, 135502 (2005).
[24] X. Xiao and L. Quian, Langmuir **16**, 8153 (2000).
[25] Water condensation can take place at distances larger than typical intermolecular distances a_0. U_{dis} would then be slightly lower than that predicted by Eqs. (2) and (4).
[26] L. Xu *et al.*, J. Phys. Chem. B **102**, 540 (1998).
[27] M. He *et al.*, J. Chem. Phys. **114**, 1355 (2001).
[28] N. A. Burham *et al.*, Nanotechnology **8**, 67 (1997).
[29] B. Gotsmann and H. Fuchs, Appl. Phys. A **72**, S55 (2001); B. Gotsmann, C. Seidel, B. Anczykowsky, and H. Fuchs, Phys. Rev. B **60**, 11 051 (1999).
[30] B. V. Dejarguin, V. M. Muller, and Y. P. Toporov, J. Colloid Interface Sci. **53**, 314 (1975).
[31] Simulation parameters: the Hamaker constant $\mathcal{A} = 6 \times 10^{-20}$ J, the effective Young modulus $E^* = 130$ GPa, $\gamma = 0.072$ N/m, $\theta_1 = \theta_2 = 0$, RH = 50%, and $R_T = 20$ nm.
[32] N. F. Martínez and R. García, Nanotechnology **17**, S167 (2006).
[33] R. García *et al.*, Phys. Rev. Lett. **97**, 016103 (2006).
[34] The exact behavior of the curves depends on the way the tip approaches the sample. The equation of motion can be solved using different initial conditions for each distance D_0 as done in Ref. [17] or, as done here, changing D_0 at a constant speed (10 nm/s). Both methods give, in general, different curves, although they present similar qualitative behaviors.
[35] S. Hu and A. Raman, Phys. Rev. Lett. **96**, 036107 (2006).